Microwave-assisted synthesis of $ZnO/ZnCo_2O_4$ heterostructure: Studies on electrochemical performance as supercapacitor electrode

S. Rajagopal [a], S. Gnanam [a*], V. Kathirvel [b], Pandiyarasan Veluswamy [c, d], S. Paulraj [e*]

[a] Department of Physics, School of Basic Sciences, Vels Institute of Science, Technology & Advanced Studies (VISTAS), Chennai-600117, India.

[b] Department of Physics and Nanotechnology, SRM Institute of Science and Technology, Kattankulathur-603203, India

[c] SMart and Innovative Laboratory for Energy Devices (SMILE), Indian Institute of Information Technology Design and Manufacturing (IIITDM) Kancheepuram, Chennai, 600127, India

[d] School of Interdisciplinary Design and Innovation (SIDI), Indian Institute of Information Technology Design and Manufacturing (IIITDM) Kancheepuram, Chennai, 600127, India

[e] Centre for Automotive Energy Materials, International Advanced Research Centre for Powder Metallurgy & New Materials (ARCI), IIT M Research Park, Chennai - 600 113, Tamil Nadu, India

[*]**Corresponding author**:gnanam.nanoscience@gmail.com, gegipaul@gmail.com

Abstract

In this study, we report the facile microwave synthesis of pure $ZnCo_2O_4$ and $ZnO/ZnCo_2O_4$ heterostructures and their electrochemical performances. In order to identify the phase, X-ray diffraction (XRD) measurement was carried out and the result confirm the cubic structure $ZnCo_2O_4$. In addition to $ZnCo_2O_4$, peaks of ZnO were identified in the spectrum which confirms the formation of heterostructures. The morphology of the prepared materials was observed by SEM and TEM analysis. The surface composition of the heterostructures was characterized by XPS technique. Cyclic voltammetry (CV) and galvanostatic charge/discharge (GCD) and electrochemical impedance spectroscopy (EIS) studies have been performed with 1 M KOH as electrolyte on the synthesised materials. The higher specific capacitance of 216 F g^{-1} at a current density of 1 A g^{-1} and an energy density of 4.8 Wh kg^{-1} at a power density of 200 W kg^{-1} was observed for $ZnO/ZnCo_2O_4$ heterostructures.

Keywords: Ternary metal oxide, heterostructures, microwave irradiation, supercapacitor, Specific capacitance

1. Introduction

Global energy crisis strive the researchers to replace the depleting fossil fuel with renewable energy sources such as solar, wind and other alternate energy sources [1]. The renewable energy sources, fuel cells, batteries and supercapacitors, are the promising technologies which have been used as power sources in electronic devices and hybrid electric vehicles to overcome the current scenario [2, 3]. The interests of studying supercapacitors have been increased due to their high-power density, long cycle life and excellent reliability [4]. Supercapacitors of carbon-based materials, conductive polymers and metal oxides have been studied extensively over the years. Intense research has been carried out on metal oxides nanomaterials such as, RuO_2, NiO, ZnO, V_2O_5, MnO_2 etc., as supercapacitor electrode due to their specific capacitance, rich redox reactions, environment friendliness and low cost [5]. Though, there is still challenge to improve the electrochemical performances of these materials because of the low electrical conductivity, poor ion diffusion rate and lack of stability which forbid them for the practical applications [6]. Recently, a new type of ternary transition metal oxides (TTMO), especially complex spinel structured cobaltite's with general formula MCo_2O_4 (M = Zn, Ni, Mn, Fe, and Cu) have displayed outstanding electrochemical performance as a pseudo-capacitive electrode material due to their coexistence of two different metal atoms in a single compound [7, 8]. Among them, $ZnCo_2O_4$, a *p*-type semiconducting metal oxide, is considered to be one of the best candidates for supercapacitor applications due to its low-cost and high specific capacitance. It is also reported that the charge storage capacity has been enhanced by the fabrication of heterostructures, dispersing two discrete metal oxide phases, such as, Co_3O_4/Fe_2O_3, $CoO/CoFe_2O_4$, $NiFe_2O_4/Fe_2O_3$ and $ZnO/ZnFe_2O_4$ [9-12]. Various synthesis methods, electro-spinning, micro-emulsion, molten-salt, hydrothermal, microwave-assisted liquid phase, chemical vapor deposition and chemical bath deposition, have been involved to grow different morphology of $ZnCo_2O_4$ for lithium-ion battery energy storage applications [13-18]. Herein, we have selected to economical microwave-irradiation method for the synthesis of $ZnO/ZnCo_2O_4$ heterostructures. There are very few reports on the microwave synthesis of $ZnCo_2O_4$ nanomaterials [19-22]. However, to the best of our knowledge, there are no reports on electrochemical investigation of $ZnO/ZnCo_2O_4$ heterostructures prepared by microwave-irradiation method. The proposed microwave-irradiation synthesis method is a facile, environment friendly and cost-effective; hence it would pave the way for real device applications.

2. Experimental

All the reagents are of analytical grade (AR) and used without further purification. Nanostructures of $ZnCo_2O_4$ and $ZnO/ZnCo_2O_4$ have been synthesized via facile, environment

friendly microwave-irradiation method. In the typical synthesis of $ZnCo_2O_4$, firstly zinc nitrate hexahydrates (2 mmol) and cobalt nitrate hexahydrate (4 mmol) were dissolved in 50 ml of mixed distilled water and ethanol (1:1 ratio) solution. Subsequently, 8 mmol of sodium hydroxide was added drop wise and stirred vigorously for 30 min using magnetic stirrer to obtain the homogeneous pink solution. The resultant solution was introduced in a household microwave oven (2.45 GHz) and irradiated with the power of 800 W for 5 min in an ambient atmosphere. After the irradiation, the product was cooled down to room temperature and then cleaned several times with ethanol and distilled water. Further, the obtained washed product was subjected to dry at 60°C in hot air oven for 12 h. Finally, the crystallinity of the synthesized powders was improved by annealing at 450°C for 5 h in the muffle furnace. To synthesis $ZnO/ZnCo_2O_4$heterostructure, similar procedure was followed with the precursors of zinc nitrate hexahydrates (3.5 mmol), cobalt nitrate hexahydrate (4 mmol) and NaOH (8 mmol).

The structural characteristics of the annealed samples were examined by powder X-ray diffraction (Bruker AXS D8 Advance model diffractometer) with Cu *K*-alpha radiation (λ = 1.5406 Å) as X-ray source. With the help of Thermo scientific Apreo S Hi-resolution scanning electron microscope (HRSEM) and JEOL/JEM 2100 transmission electron microscope (TEM) the morphology and elemental composition of the samples were studied. In order to study the surface elemental compositions, X-ray photoelectron spectroscopy (XPS, PHI Versaprobe III) with Al-*K*α monochromatic radiation analysis was carried out.

Electrochemical performance of the synthesized nanomaterials was investigated in 1M KOH electrolyte in the potential range of 0 to 0.4 V. The working electrodes were prepared by coating the synthesized $ZnCo_2O_4$ and $ZnO/ZnCo_2O_4$ nanoparticles on to the ultrasonically cleaned nickel foam (1×1 cm). Initially, the slurry was prepared by mixing the active material, activated carbon and polyvinylidene fluoride in a ratio of 85:15:5 with N-methyl-2-pyrrolidone solvent. The resulting slurry was applied uniformly on the nickel foam and allowed to dry at 60 ºC for 24 h. The electrochemical studies were performed in BioLogic SP3 electrochemical workstation by following a three-electrode system: fabricated electrode as working electrode, Ag/AgCl as reference electrode and platinum wire as the counter electrode.

3. Results and Discussion

Powder X-ray diffraction analysis shows the crystal structure and purity of the synthesized nanoparticles. Fig. 1 (a-b) represents the XRD pattern of $ZnCo_2O_4$ nanoparticles and $ZnO/ZnCo_2O_4$ heterostructures. Fig. 1a shows that all the diffraction peaks are well indexed to the cubic spinel structure of $ZnCo_2O_4$ according to the JCPDS No: 23-1390. Fig. 1b shows the XRD pattern of $ZnO/ZnCo_2O_4$ heterostructures. It is noted that there were additional peaks along with $ZnCo_2O_4$ and they are assigned to the hexagonal structure of ZnO (JCPDS No: 36-1451) which confirms the formation of heterostructures. The strong and

sharp peaks show that the crystallized samples were well ordered and no other impurity peaks occurred.

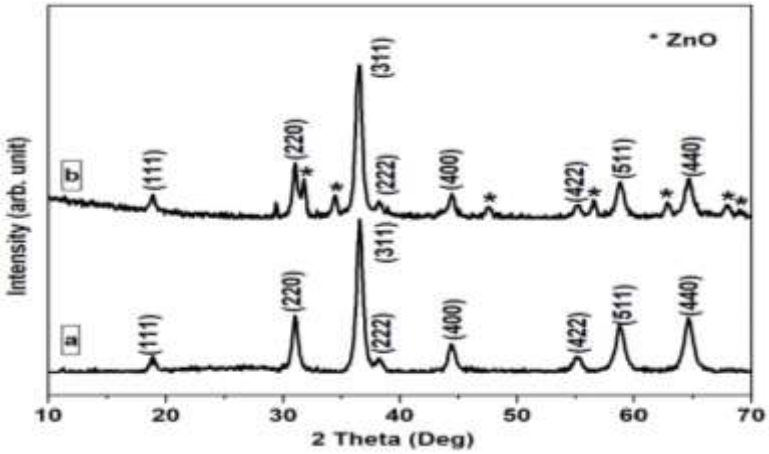

Fig. 1 XRD pattern of $ZnCo_2O_4$ and $ZnO/ZnCo_2O_4$ nanoparticles

The morphology of the samples was studied by HR-SEM analysis. Fig. 2 (a-b) shows the HR-SEM images of pure $ZnCo_2O_4$ and $ZnO/ZnCo_2O_4$ heterostructures at different magnification. It is observed that the pure $ZnCo_2O_4$ nanoparticles are interconnected and formed porous nanosheet-like morphology with some vertically grown nanoparticles. The heterostructures morphology is similar to the pure $ZnCo_2O_4$ with suppressed growth in the vertical direction.

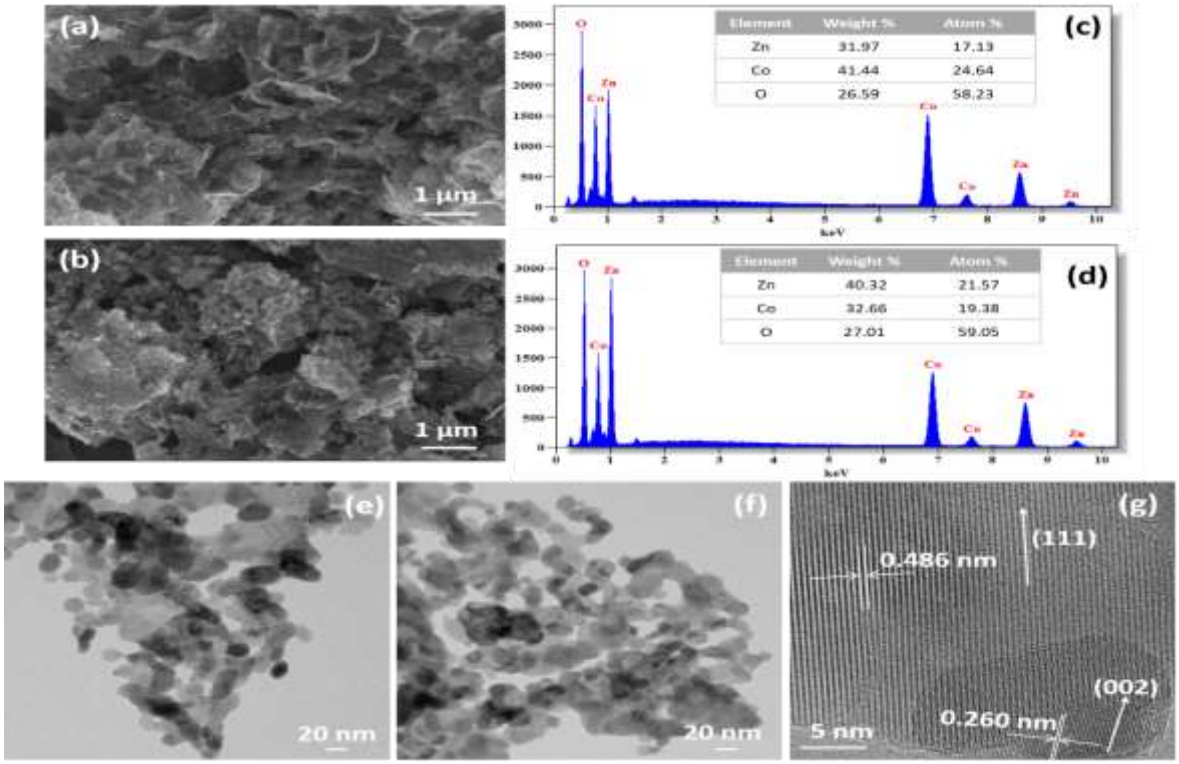

Fig. 2HR-SEM of (a) $ZnCo_2O_4$ (b)$ZnO/ZnCo_2O_4$, EDAX spectrum of (c) $ZnCo_2O_4$ (d) $ZnO/ZnCo_2O_4$,TEM images of (e) $ZnCo_2O_4$ and(f) $ZnO/ZnCo_2O_4$, (g) HR-TEM of $ZnO/ZnCo_2O_4$

The elmental composition of the synthesized samples were analysed using Energy Dispersive X-Ray spectroscopy (EDX) and is shown in Fig. 2 (c-d). It is understood from the study that the composition of Zn:Co:O was found approximately to be 1:2:4 for the pure $ZnCo_2O_4$. Theheterostructure composition revealed the excess of Zn which employes in the formation ZnO nanoparticles. TEM measurements were involved further to investigate the morphology of the prepared samples. Fig. 2 (e-f) shows the TEM image of pure $ZnCo_2O_4$ and $ZnO/ZnCo_2O_4$and it clearly identifies the porous nature of the samples. It is noted that the addition of ZnO has no impact on the morphology of the resultant material. The interplanar *d*-spacing was obtained by measuring the distance between the two adjacent lattice fringes and it is displayed in Fig. 2g. The measured values are 0.486 nm and 0.260 nm and they could be assigned to (111) plane of $ZnCo_2O_4$ and (002) plane of ZnO, respectively.

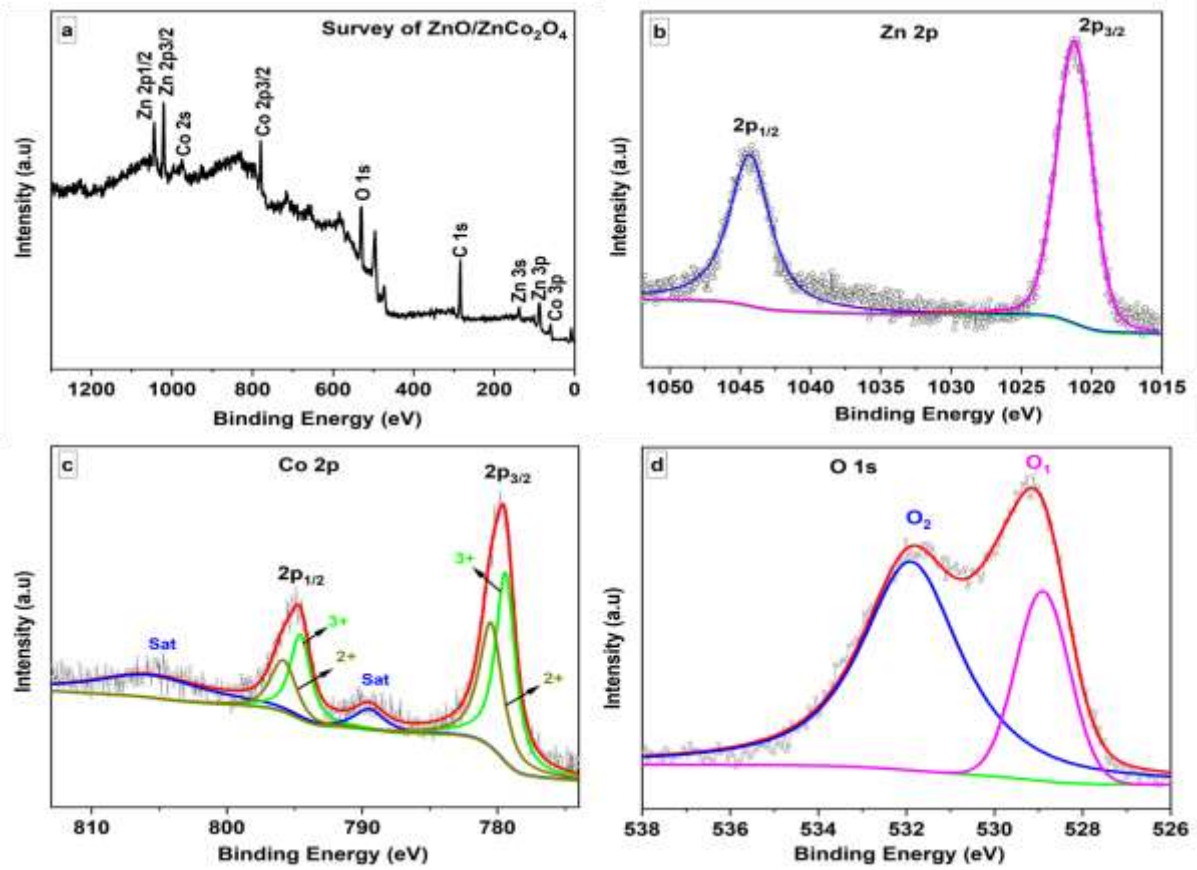

Fig. 3 XPS analysis of $ZnO/ZnCo_2O_4$. (a) XPS survey spectrum of $ZnO/ZnCo_2O_4$. (b) Zn 2*p*, (c) Co 2*p*, and (d) O 1*s* binding energies.

XPS analysis was carried out in order to investigate the surface chemical composition and oxidation states of metals present in $ZnO/ZnCo_2O_4$. Fig. 3a shows the survey spectrum of $ZnO/ZnCo_2O_4$ and it is clearly seen that the presence of Ni, Co, O and C in the spectrum. Narrow scan measurement was employed further to examine the oxidation states of Zn, Co, and O ions. The existence of Zn^{2+} states was confirmed from the high-resolution spectra of Zn 2*p* in which two characteristics peaks such as, $2p_{3/2}$ and $2p_{1/2}$ were observed at 1021 and 1044

eV, respectively (Fig. 3b) and they are in well accordance with the reported values [23].In the high-resolution spectra of Co 2*p*, two spin-orbit doublets, corresponds to Co^{2+} and Co^{3+}, and two satellite peaks were appeared. The two spin-orbit doublets are assigned to Co^{2+} at binding energies of 780.5 and 796 eV while the other two doublet peaks are ascribed to Co^{3+} at binding energies of 779.5 and 794.5 eV. The observed Co 2*p* peaks are in good agreement with the literature [24].The two supplementary peaks at 789.5 and 806 eV are interpreted as satellite peaks indicated as "sat". The deconvoluted O 1s spectra could be fitted with two peaks at 529 eV and 532 eV. The fitted peak at 529 eV is ascribed to metal-oxygen bonds while the peak at 532 eV is associated with chemisorbed oxygen species.

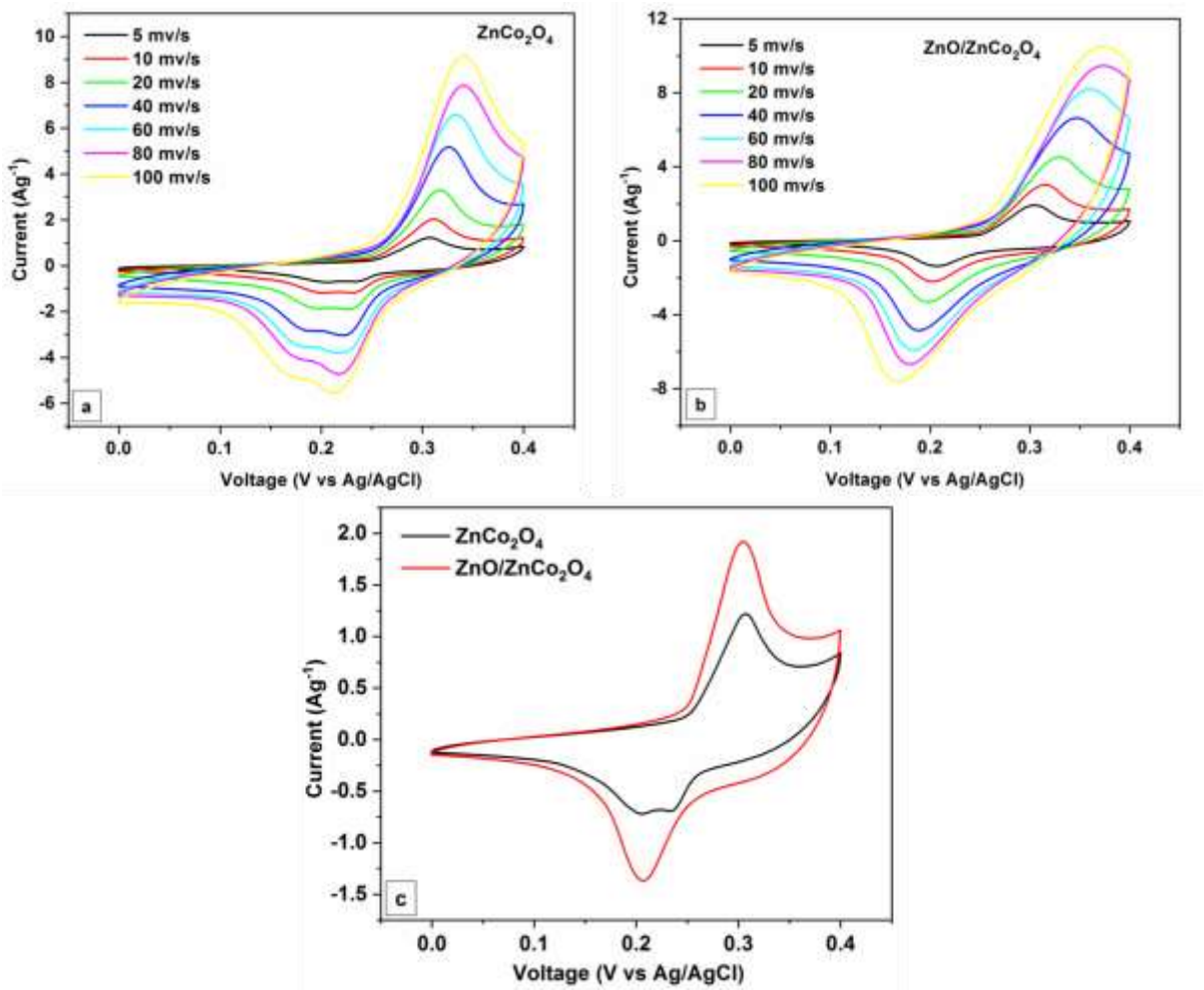

Fig. 4 CV curve of (a) $ZnCo_2O_4$, (b) $ZnO/ZnCo_2O_4$ at different scan rates 5-100 mVs^{-1} and (c) Comparison of CV profile $ZnCo_2O_4$ and $ZnO/ZnCo_2O_4$ at a scan rate of 5 mVs^{-1}.

The electrochemical properties of the prepared samples were investigated by CV, GCD and EIS measurements in 1 M KOH aqueous electrolyte using a three-electrode configuration. The specific capacitance is due to the insertion of extraction of K^+ ion from the electrolyte into the pores of working electrode. $ZnCo_2O_4$ and $ZnO/ZnCo_2O_4$ electrode in the KOH electrolyte exhibit very good capacitance, energy density and power density values. Fig. 4

(a-b) depicts the CV curves drawn for $ZnCo_2O_4$ and $ZnO/ZnCo_2O_4$ electrodes in the potential range between 0 and 0.4 V (vs Ag/AgCl) at scan rates from 5 to 100 mVs^{-1}.

The CV profile for all the scan rates exhibits redox peaks, which is from the reversible faradic reactions of Zn–O/Zn–O–OH and Co–O/Zn–O–OH associated with OH^- anions, confirming the capacitance is due to the pseudocapacitive mechanism in the metal oxide system. The CV profile is well preserved while increasing the scan rate which implies that the rate capability and mass transport are excellent in the electrode. However, there is a slight shift in the anodic and cathodic peak currents towards higher and lower potential due to the internal resistance and polarization effect of the electrode. Fig. 4c compares the CV profile of $ZnCo_2O_4$ and $ZnO/ZnCo_2O_4$ at 5 mVs^{-1}. It is clearly seen that the integrated area of $ZnO/ZnCo_2O_4$ is greater than that of $ZnCo_2O_4$, denoting that the heterostructures holds high specific capacitance than the pure $ZnCo_2O_4$.

Fig. 5 (a-b) represents the GCD curves of $ZnCo_2O_4$ and $ZnO/ZnCo_2O_4$ electrodes at various current densities (1, 2, 4, 6, 8 and 10 Ag^{-1}) in the potential range of 0 to 0.4 V. The deviation of the GCD curve from the straight and flat line indicates that the capacitance of the materials is mainly from the redox reaction and it is consistent with the CV profile. The discharge GCD curve can be divided into two segments: 0.4 – 0.25 V and 0.25 – 0 V (vs Ag/AgCl). The potential changes very rapidly with respect to time in the first segment (0.4 – 0.25 V) due to the pure EDLC capacitance on the electrode/electrolyte interface by the charge separation which results in a short discharge time. In the second segment (0.25 – 0 V), the voltage changes very slowly with respect to time indicating that the capacitance is due to the redox reaction on the electrode/electrolyte interface and the discharge time is longer than the former segment. The specific capacitance (*C*s) can be calculated using the following formula,

$$C_s = \frac{I\,\Delta t}{m\,\Delta V}$$

Where I – the discharge current, Δt – the discharge time, m – mass of the active materials in the electrode, and ΔV – the potential window. The calculated specific capacitances are 128, 94, 66, 54 and 45 Fg^{-1} for pure $ZnCo_2O_4$ and 216, 192, 154, 127, 109 and 95 Fg^{-1} for $ZnO/ZnCo_2O_4$ at a current density of 1, 2, 4, 6, 8 and 10 Ag^{-1}, respectively.

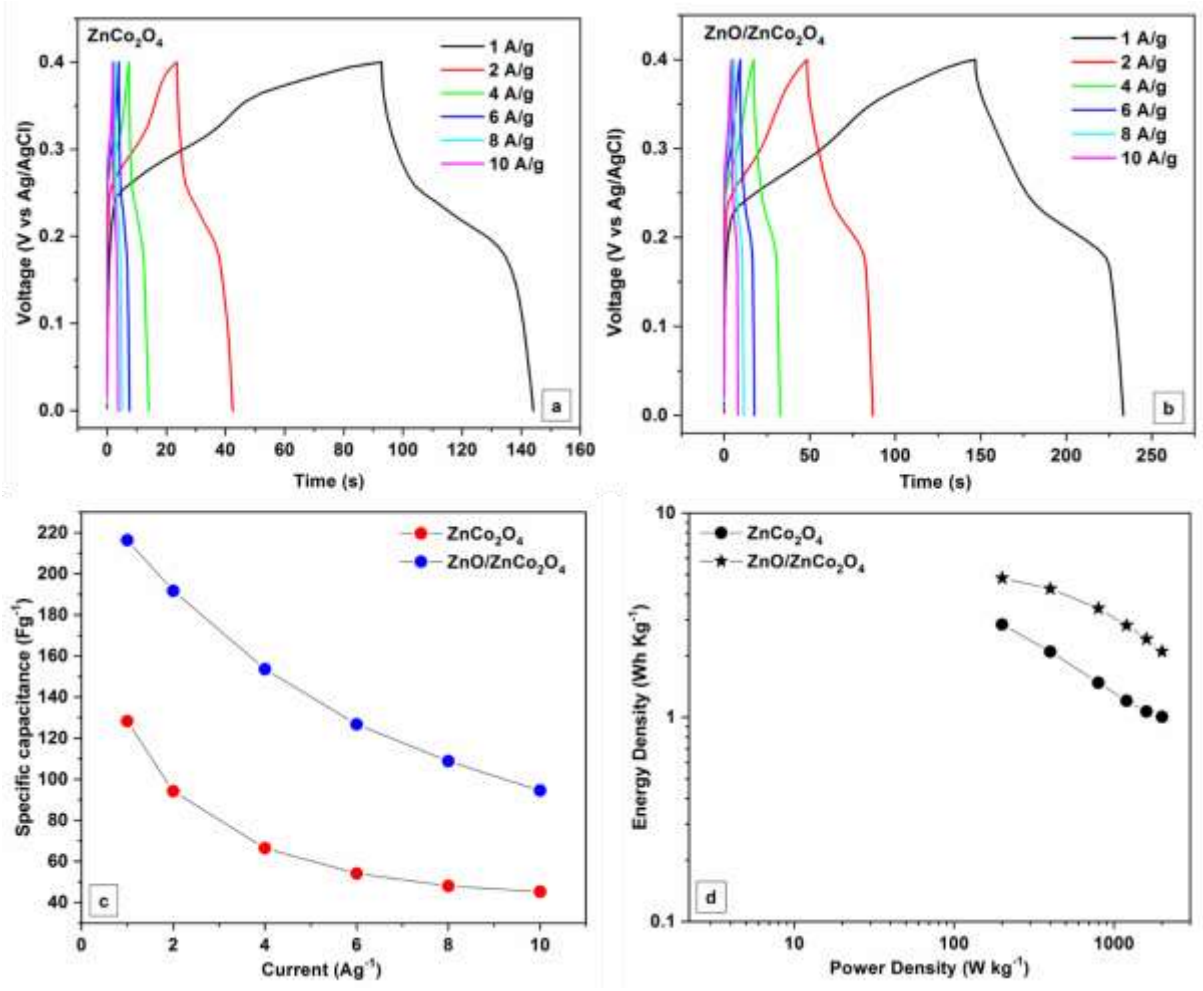

Fig. 5(a-b) Galvanometric charge/discharge curves of $ZnCo_2O_4$ and $ZnO/ZnCo_2O_4$ electrodes, respectively, (c) Comparison of specific capacitance at various current density of $ZnCo_2O_4$ and $ZnO/ZnCo_2O_4$ and (d) Ragone plot of pure $ZnCo_2O_4$ and $ZnO/ZnCo_2O_4$

The heterostructures showed high specific capacitance than the pure $ZoCo_2O_4$ for all the current densities, proved that the formation of heterostructures enhances the electrochemical performance. Upon increasing current density, the specific capacitance decreases gradually for both the cases (Fig. 5c). Ragone plots (Fig. 5d) were drawn by calculating the energy and power densities at various current densities from the GCD curve. To investigate the electrochemical performance further the energy and power density have been determined for $ZnCo_2O_4$ and $ZnO/ZnCo_2O_4$ from the following equations:

$$E = \frac{1}{2} C_s V^2$$

$$P = \frac{E}{\Delta t}$$

The calculated energy density is 2.8 and 4.8 $Whkg^{-1}$ at a power density of 200 Wkg^{-1} for $ZnCo_2O_4$ and $ZnO/ZnCo_2O_4$, respectively.

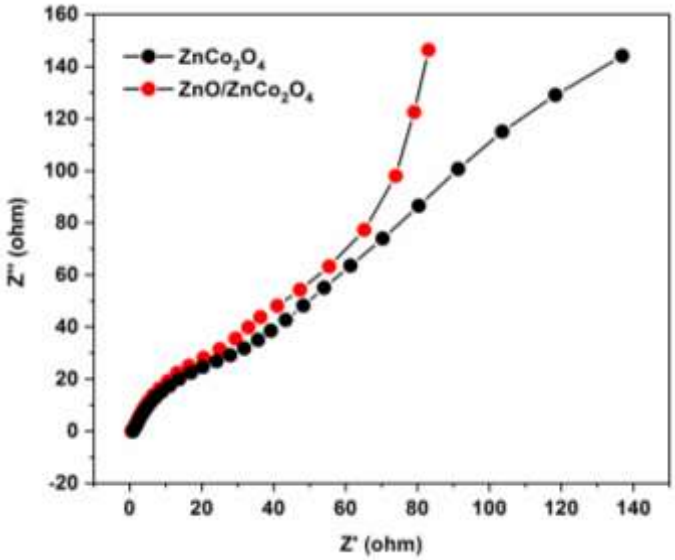

Fig.6 Nyquist plot of $ZnCo_2O_4$ and $ZnO/ZnCo_2O_4$ electrodes.

Electrochemical impedance was studied in the 0.1 MHz to 1 Hz frequency range in order to investigate the electrical conductivity of the samples. Fig. 6 represents the impedance curves for $ZnCo_2O_4$ and $ZnO/ZnCo_2O_4$ electrodes. The impedance $Z(\omega)$ is composed of a real (Z') and an imaginary part (Z") and they are plotted on the x-axis and y-axis, respectively, to get a Nyquist plot. There is no well-defined semi-circle in the high-medium frequency region which signifies the fast electron transfer rate at the electrode/electrolyte interface and high electronic conductivity [25]. A straight line at the low frequency region originated from Warburg impedance and it is steeper along the imaginary axis for $ZnO/ZnCo_2O_4$, indicating the smaller diffusion resistance than the pure $ZnCo_2O_4$. The Z' intercept gives the bulk electrolyte resistance in the high frequency region and it is found to be 0.8 and 0.5 Ω, respectively for $ZnCo_2O_4$ and $ZnO/ZnCo_2O_4$.

4. Conclusions

In summary, $ZnCo_2O_4$ and $ZnO/ZnCo_2O_4$ were successfully synthesized via facile microwave irradiation method and examined their electrochemical performances as supercapacitor anode material. The structural characterization, XRD, confirmed the formation of $ZnO/ZnCo_2O_4$ heterostructures whereas $ZnCo_2O_4$ and ZnO crystallize in cubic and hexagonal, respectively. Morphological analysis HR-SEM and TEM revealed the porous nature of the synthesise materials. Addition of ZnO has no influnce in the morphology of $ZnCo_2O_4$. Typical redox peaks were observed for both the pure $ZnCo_2O_4$ and $ZnO/ZnCo_2O_4$ samples. Compared to pure $ZnCo_2O_4$, the larger specific capacitance of 216 F g^{-1} at a current density of 1 A g^{-1} was obtained for $ZnO/ZnCo_2O_4$ heterostructures from the GCD measurement. The energy density was found to be 4.8 Wh kg^{-1} at a power density of 200 W kg^{-1} for $ZnO/ZnCo_2O_4$ heterostructures. The investigations on the $ZnO/ZnCo_2O_4$ heterostructures suggest that the environment friendly facile microwave synthesized composite can be a promising anode material for supercapacitor application.

Acknowledgments

One of the authors, Pandiyarasan Veluswamy, would like to thank the Innovation in Science Pursuit for Inspired Research (INSPIRE) Faculty Program through the Department of Science and Technology (DST) funded by the Ministry of Science and Technology (DST/INSPIRE/04/2017/ 002629).

References

1. Z. Bi, Q. Kong, Y. Cao, G. Sun, F. Su, X. Wei, X. Li, A. Ahmad, L. Xie, C. M. Chen, J. Mater. Chem. A,7, 16028 (2019).
2. C. Chen, C. Ai, Y. He, S. Yang, Y. Wu, J. Alloy. Compd.705, 438 (2017).
3. C. An, Y. Zhang, H. Guo and Y. Wang, Nanoscale Adv., 1, 4644 (2019).
4. L. Li, H. Bi, S. Gai, F. He, P. Gao, Y. Dai, X. Zhang, D. Yang, M. Zhang, P. Yang, Sci. Rep.,7, 43116 (2017).
5. W. W. Liu, C. Lu, K. Liang, B. K. Tay, J. Mater. Chem. A, 2, 5100 (2014).
6. Y. Gai, Y. Shang, L. Gong, L.Su, L. Hao, F. Dong, J. Li, RSC Adv., 7, 1038 (2017).
7. B. Liu, B. Liu, Q. Wang, X. Wang, Q. Xiang, D. Chen, G. Shen, ACS Appl. Mater. Interfaces, 5, 20, 10011 (2013).
8. D. Chen, Q. Wang, R. Wang, G. Shen J. Mater. Chem. A, 3(19), 10158 (2015).
9. Z. Li, B. Li, L. Yin, Y. Qi, ACS Appl. Mater. Interfaces, 6, 11, 8098 (2014).
10. M. X. Li, Y. X. Yin, C. J. Li, F. Z. Zhang, L. J. Wan, S. L. Xu, D. G. Evans, Chem. Commun., 48, 410 (2012).
11. G. Huang, F. F. Zhang, L. L. Zhang, X. C. Du, J. W. Wang, L. M. Wang, J. Mater. Chem. A, 2, 8048 (2014).
12. S. K. Jhajharia, Z. Manappadan, K. Selvaraj, Chem. Electro. Chem., 6, 1 (2019)
13. W. Luo, X. Hu, Y. Sun, Y. Huang, J. Mater. Chem., 22, 8916 (2012).
14. N. Du, Y. Xu, H. Zhang, J. Yu, C. Zhai, D. Yang, Inorg. Chem., 50, 3320 (2011).
15. M. V. Reddy, K. Y. H. Kenrick, T. Y. Wei, G. Y. Chong, G. H. Leong, B. V. R. Chowdari, J. Electrochem, Soc., 158, 12, A1423 (2011).
16. H. Liu, J. Wang, Electrochim. Acta, 92, 371 (2013).
17. Y. Zhu, C. Cao, J. Zhang, X. Xu, J. Mater. Chem. A, 3, 9556 (2015).
18. H. Chen, Q. Zhang, J. Wang, Q. Wang, X. Zhou, X. Li, Y. Yang, K. Zhang, Nano Energy 10, 245 (2014).
19. P. Huang, M. Zhang, J. Kang, H. Feng, Q. Su, G. Du, Y. Yu, B. Xu, J. Mater. Sci.,5, 4154 (2019).
20. G. H. Shih, W. R. Liu, RSC Adv., 7, 42476 (2017).
21. Y. Wang, K. Jun, Y. Zhang, Y. Huang, J. Mater. Chem. A, 3, 24303 (2015).
22. T.V.M. Sreekanth, R. Ramaraghavulu, S.V. Prabhakar Vattikuti, J. Shim, K. Yoo, Mater. Lett., 253, 450 (2019).

23. J. Li, J. Wang, D. Wexler, D. Shi, J. Liang, H. Liu, S. Xiong, Y. Qian, J. Mater. Chem. A, 1, 1522 (2013)
24. Y. Li, N. Luo, G. Sun, B. Zhang, H. Jin, L. Lin, H. Bala, J. Cao, Z. Zhang, Y. Wang, Sens. Actuators B Chem., 287, 199 (2019)
25. H. Niu, X. Yang, H. Jiang, D. Zhou, X. Li, T. Zhang, J. Liu, Q. Wang, F. Qu, J. Mater. Chem. A, 3, 24082(2015).